RAA 2015 Vol. **15** No. **4**, 597–607 doi: 10.1088/1674–4527/15/4/011
http://www.raa-journal.org *http://www.iop.org/journals/raa*

Research in Astronomy and Astrophysics

Asteroid body-fixed hovering using nonideal solar sails

Xiang-Yuan Zeng, Fang-Hua Jiang and Jun-Feng Li

School of Aerospace Engineering, Tsinghua University, Beijing 100084, China;
jiangfh@tsinghua.edu.cn

Received 2014 May 22; accepted 2014 July 21

Abstract The problem of body-fixed hovering over an asteroid using a compact form of nonideal solar sails with a controllable area is investigated. Nonlinear dynamic equations describing the hovering problem are constructed for a spherically symmetric asteroid. Numerical solutions of the feasible region for body-fixed hovering are obtained. Different sail models, including the cases of ideal, optical, parametric and solar photon thrust, on the feasible region is studied through numerical simulations. The influence of the asteroid spinning rate and the sail area-to-mass ratio on the feasible region is discussed. The required orientations for the sail and their corresponding variable lightness numbers are given for different hovering radii to identify the feasible region of the body-fixed hovering. An attractive scenario for a mission is introduced to take advantage of solar sail hovering.

Key words: space vehicles: celestial mechanics — cosmology: observations

1 INTRODUCTION

Missions that explore hazardous asteroids that might come close to Earth (Scheeres 2004) have been frequently investigated as a precursor to some mitigation strategy or a controlled landing. According to previous studies, there are a number of possible options for explorations in the vicinity of an asteroid, including a Sun-synchronous orbit (Morrow et al. 2001), a retrograde orbit (Broschart & Scheeres 2005) or a heliostationary orbit (Morrow et al. 2002) in which a spacecraft is placed at the libration point (Baoyin & McInnes 2005) of a system. Besides these methods, the spacecraft could also maintain a required fixed position relative to the rotating asteroid in a configuration referred to as "body-fixed hovering." This has been proposed as an effective way for a human landing on an asteroid or a sample return mission which was successfully accomplished by *Hayabusa* (Scheeres 2004). If the mission requires prolonged observation of a specific area from a position away from synchronous orbit, the application of thrust must consider both gravitational and centrifugal forces. Thus, the extended period of hovering will greatly depend on the onboard supplies of fuel for a chemical or continuous low-thrust spacecraft. Compared to a conventional spacecraft, the inherent capabilities of solar sailing, which does not consume fuel, make this approach well suited for exploring asteroids.

Orbital dynamics close to an asteroid is quite challenging and complex due to their irregular shape and rotation (Hu & Scheeres 2008; Li et al. 2013). Additionally, solar radiation pressure (SRP) becomes a significant perturbing force in the vicinity of small asteroids (Scheeres 1999). Another advantage of solar sailing is to utilize the SRP force as an active control. The first detailed

analysis of sail operations applied to asteroids was made by Morrow et al. (2001). Sawai et al. (2002) and Broschart & Scheeres (2005) investigated body-fixed hovering with conventional propulsion systems. Zhang et al. (2013) extended such hovering from the case of a satellite near an asteroid to two satellites near each other. However, body-fixed hovering over an asteroid by using a solar sail was not addressed before Williams & Abate (2009). In their work, a model of an ideally reflecting sail with an associated sail efficiency factor (to reflect the difference between a true sail and an ideal one) was adopted. The corresponding SRP force was normal to the sail's surface. Nonideal sails have not yet been discussed in the context of body-fixed hovering above an asteroid, although approaches to heliostationary flights have been presented by Morrow et al. (2002) and Farrés & Jorba (2012).

Use of a solar sail has been seriously considered as an alternative propulsion system since the proposed Comet Halley rendezvous mission. A number of demonstrative missions (McInnes 1999; Baoyin & McInnes 2006) have been investigated along with their corresponding practical experiments. Some dramatic mission concepts involving non-Keplerian orbits (Gong et al. 2007, 2009a; Vulpetti 1997) have been proposed that incorporate a solar sail. The successful flight of IKAROS and *NanoSail-D2* have gained a lot of interest from the space community and laid the first stone for further missions that utilize solar sails (Gong et al. 2011). The concept of a furlable solar sail was proposed by Williams & Abate (2009) to generalize the feasible region where body-fixed hovering can occur. Compared to a fixed-area solar sail with two variable attitude angles, the essence of a furlable sail is to separate the maximum magnitude of the SRP force as an independent control variable. Such a performance can also be implemented with a variable reflectivity sail film to control the sail attitude, which was partially demonstrated on IKAROS.

In this paper, a compact form of nonideal sails (Mengali & Quarta 2007) with a controllable sail area is adopted to accomplish body-fixed hovering near an asteroid. A comparison is made to quantify the influence of the four different sail models (including ideal-, optical-, parametric- and solar photon thrust) on the hovering scenarios. For the target asteroid, a spherically symmetric model is applied as an estimation of the first step. The asteroid model can be relaxed and extended in future studies. The analysis presented here complements studies made by Williams & Abate (2009) and is extended to scenarios with realistic sails. Section 2 gives the equations of the body-fixed hovering problem in terms of the compact sail model. In Section 3 the effects of the asteroid's spinning and the sail's area-to-mass ratio on body-fixed hovering is also illustrated via numerical simulations. Moreover, sail control profiles corresponding to different hovering radii are presented to identify the feasibility of body-fixed hovering by using a solar sail. Conclusions are given in Section 4.

2 FORMULATION OF BODY-FIXED HOVERING

2.1 Equations of Motion

In this analysis, a two-body gravitational model is adopted to describe the dynamics of the spacecraft near an asteroid. The vector dynamical equation for a solar sail in the uniformly rotating body-fixed coordinate frame *oxyz* (Scheeres et al. 1998) can be written as

$$\frac{d^2\boldsymbol{r}}{dt^2} + 2\boldsymbol{\omega} \times \frac{d\boldsymbol{r}}{dt} + \boldsymbol{\omega} \times (\boldsymbol{\omega} \times \boldsymbol{r}) = \boldsymbol{a}_{\mathrm{SRP}} - \frac{\partial U(\boldsymbol{r})}{\partial \boldsymbol{r}}, \tag{1}$$

where $\boldsymbol{r}$ is the position vector from the asteroid's center of mass to the sailcraft, $\boldsymbol{\omega}$ is the rotational angular velocity vector of the asteroid with respect to the inertial reference frame *IXYZ*, $U(\boldsymbol{r})$ is the gravitational potential of the asteroid and $\boldsymbol{a}_{\mathrm{SRP}}$ is acceleration from the non-conservative SRP. The coordinate system *IXYZ* centered on the asteroid is shown in Figure 1. The + *IZ* axis is along the direction of the asteroid's angular velocity, the +*IX* axis is along the anti-solar direction and in the asteroid's equatorial plane, and the +*IY* axis is also in the asteroid's equatorial plane making up an orthogonal right-handed triad. Strictly speaking, the inertial frame *IXYZ* is a nearly non-rotating coordinate system due to the conic motion of the asteroid. However, compared to the spinning period

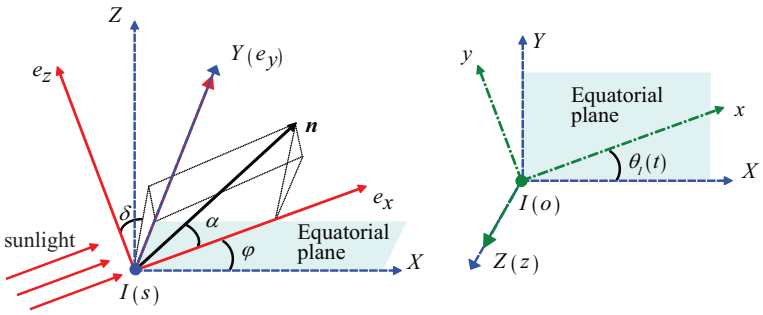

Fig. 1 Orbital reference frames and sail attitude angles.

of the asteroid, which is on the order of hours to days at most, the rotation of the frame *IXYZ* is on the order of a thousand days beyond 2 AU away from the Sun. Thus, for those asteroids in the main belt, the frame *IXYZ* can be treated as an inertial reference frame.

The body-fixed frame *oxyz* coincides with the frame *IXYZ* at the initial time and the transformation matrix from *oxyz* to *IXYZ* is

$$C_1(t) = \begin{bmatrix} \cos\theta_1 & -\sin\theta_1 & 0 \\ \sin\theta_1 & \cos\theta_1 & 0 \\ 0 & 0 & 1 \end{bmatrix}, \tag{2}$$

where the angle $\theta_1(t) = \omega t$ and ω is the scalar orbital angular velocity. In order to express the SRP force, a coordinate system for incident light $se_xe_ye_z$, shown in Figure 1, is established where the $+se_x$ axis is along the direction of sunlight. The axis $+se_y$ coincides with the *+IY* axis and se_z completes the right-handed frame. In this frame, the unit vector $\boldsymbol{s}$ directed from the Sun to the asteroid is always $[1, 0, 0]^{\mathrm{T}}$, which is the same as the unit vector of the axis $+se_x$. If there is a solar latitude angle φ between the sunlight and the asteroid's equatorial plane, the transformation matrix from *IXYZ* to $se_xe_ye_z$ is

$$C_2 = \begin{bmatrix} \cos\varphi & 0 & \sin\varphi \\ 0 & 1 & 0 \\ -\sin\varphi & 0 & \cos\varphi \end{bmatrix}, \ \varphi \in \left[-\frac{\pi}{2}, \frac{\pi}{2}\right]. \tag{3}$$

As seen from Figure 1, if axis $+se_x$ is along axis *+IZ* corresponding to $\varphi = \pi/2$, the Sun is located at the south pole of the asteroid. If $\varphi = 0$, the sunlight is parallel to the asteroid's equatorial plane.

2.2 Force Model for a Solar Sail

A unified, compact design for solar sails with a fixed sail area has been presented by Mengali & Quarta (2007) to carry out advanced heliostationary missions. Compared to an ideal sail with a perfectly flat reflective surface, the optical model takes the effect of reflection, absorption and reradiation into account. The parametric model considers the billowing of the sail. Additionally, the solar photon thrust (SPT, detailed by Guerman et al. 2010) is also included in the model. The acceleration resulting from a sail with variable area can be written as

$$\boldsymbol{a}^s(t) = \frac{\beta(t)}{2} \cdot \frac{\mu_{\mathrm{Sun}}}{R_{\mathrm{AU}}^2} \cdot \cos^{(p-q)}\alpha \cdot \left[(1-q)\, b_1 \cdot \boldsymbol{e}_x^s + \left(q b_1 + b_2 \cos^{(3q+1)}\alpha + b_3 \cos^{2q}\alpha\right) \cdot \boldsymbol{n}^s\right], \tag{4}$$

where the superscript '*s*' indicates that the vector is expressed in the $se_xe_ye_z$ frame. In the above equation, $\mu_{\rm Sun}$ is the solar gravitational constant ($1.3271244 \times 10^{20}\,{\rm m^3 s^{-2}}$) and $R_{\rm AU}$ is the Sun-asteroid heliocentric distance in the unit of AU ($1\,{\rm AU} \approx 1.496 \times 10^{11}{\rm m}$). The coefficients [$p$, q, b_1, b_2, b_3] corresponding to different sail models are specified in Table 1 (but see discussions by Mengali & Quarta 2007).

Table 1 Four Different Groups of Solar Sail Force Model Coefficients

	p	q	b_1	b_2	b_3
Ideal	1	0	0	2	0
Optical	1	0	0.1728	1.6544	–0.0109
Parametric	1	1	–0.5885	–0.1598	2.5646
SPT	0	0	0	2	0

The sail cone angle α, shown in Figure 1, is defined as the angle between the sail's normal vector $\boldsymbol{n}$ and the incident light $\boldsymbol{e}_x$ ($\boldsymbol{e}_x^s = [1,\,0,\,0]^{\rm T}$) for both ideal and optical models. However, for the parametric and SPT sails, α is the angle between the SRP force and the vector $\boldsymbol{e}_x$. The orientation of the sail can be explicitly expressed as

$$\boldsymbol{n}^s = \begin{bmatrix} \cos\alpha \\ \sin\alpha\sin\delta \\ \sin\alpha\cos\delta \end{bmatrix},\ \begin{cases} \alpha \in [0,\,\pi/2] \\ \delta\ \in [0,\,2\pi) \end{cases} \tag{5}$$

where δ is the clock angle shown in Figure 1, defined as the angle between the projected line of incident light onto the plane se_ye_z and axis $+se_z$. For an ideal sail, Equation (4) becomes

$$\boldsymbol{a}^s\,(t) = \beta\,(t) \cdot \frac{\mu_{\rm Sun}}{R_{\rm AU}^2} \cdot \cos^2\alpha \cdot \boldsymbol{n}^s, \tag{6}$$

where the sail lightness number $\beta(t)$ is the ratio of the SRP acceleration to the local solar gravitational acceleration, which only depends on the area-to-mass ratio for the sail $\sigma(t)$

$$\beta\,(t) = \frac{\sigma_{\rm SL}}{\sigma\,(t)} = \frac{\sigma_{\rm SL}}{m/A(t)}, \quad \beta \le \beta_{\max}, \tag{7}$$

where the critical sail loading parameter $\sigma_{\rm SL}$ is a constant whose value is approximately $1.53\,{\rm g\,m^{-2}}$, m is the total mass of the spacecraft that uses the solar sail and $A(t)$ is the effective reflective surface of the sail. Here, $\beta_{\max}$ is the maximum available lightness number, which is a key design parameter for a mission.

2.3 Body-Fixed Hovering

The equations describing body-fixed hovering lead to a fixed equilibrium point in the frame *oxyz* at a desired position. From Equation (1), the acceleration that results from SRP should be

$$\boldsymbol{a}_{\rm SRP} = \frac{\partial U\,(\boldsymbol{r})}{\partial \boldsymbol{r}} + \boldsymbol{\omega} \times (\boldsymbol{\omega} \times \boldsymbol{r}) = \begin{bmatrix} U_x \\ U_y \\ U_z \end{bmatrix} - \begin{bmatrix} \omega^2 & 0 & 0 \\ 0 & \omega^2 & 0 \\ 0 & 0 & 0 \end{bmatrix} \begin{bmatrix} x \\ y \\ z \end{bmatrix}. \tag{8}$$

The desired position can be expressed by the latitude angle $\lambda \in [-\pi/2,\,\pi/2]$ and the longitude angle $\theta_0 \in [0,\,2\pi]$ as

$$\boldsymbol{r} = \begin{bmatrix} x \\ y \\ z \end{bmatrix} = r \begin{bmatrix} \cos\lambda\cos\theta_0 \\ \cos\lambda\sin\theta_0 \\ \sin\lambda \end{bmatrix}, \tag{9}$$

where r is the magnitude of the position vector. It is assumed here that the asteroid is spherically symmetric. Consequently, the gravitational acceleration exerted on the spacecraft is

$$\frac{\partial U(\boldsymbol{r})}{\partial \boldsymbol{r}} = \begin{bmatrix} U_x \\ U_y \\ U_z \end{bmatrix} = \frac{\mu_{\rm ast}}{r^3}\boldsymbol{r} = \frac{\mu_{\rm ast}}{r^2}\begin{bmatrix} \cos\lambda\cos\theta_0 \\ \cos\lambda\sin\theta_0 \\ \sin\lambda \end{bmatrix}, \tag{10}$$

where $\mu_{\rm ast}$ is the gravitational constant of the asteroid. Substituting Equations (9) and (10) into Equation (8), the acceleration produced by the sail is

$$\boldsymbol{a}_{\rm SRP} = \left[\left(\tfrac{\mu_{\rm ast}}{r^2} - \omega^2 r\right)\cos\lambda\cos\theta_0,\ \left(\tfrac{\mu_{\rm ast}}{r^2} - \omega^2 r\right)\cos\lambda\sin\theta_0,\ \tfrac{\mu_{\rm ast}}{r^2}\sin\lambda \right]^{\rm T}. \tag{11}$$

A constraint on the solar sail is that the SRP force can only be produced in the anti-solar hemisphere. Therefore, acceleration from the sail must satisfy

$$\left(\boldsymbol{a}^s_{\rm SRP}\right)^{\rm T}\cdot \boldsymbol{e}^s_x = \left(C_2\cdot C_1\left(t\right)\cdot \boldsymbol{a}_{\rm SRP}\right)^{\rm T}\cdot \boldsymbol{e}^s_x \geq 0. \tag{12}$$

Substituting Equations (2) and (3) into Equation (12), one can obtain

$$\left(\boldsymbol{a}^s_{\rm SRP}\right)^{\rm T}\cdot \boldsymbol{e}^s_x = \left(\frac{\mu_{\rm ast}}{r^2} - \omega^2 r\right)\cos\lambda\cos\varphi\cos\theta + \frac{\mu_{\rm ast}}{r^2}\sin\lambda\sin\varphi \geq 0, \tag{13}$$

where $\theta(t) = \theta_0 + \theta_1(t) = \theta_0 + \omega t$. Since body-fixed hovering of a solar sail occurs during the entire period of asteroid rotation, the angle $\theta(t)$ takes all values from 0 to 2π. In order to guarantee that the value of Equation (13) is always positive, the second term on the right, $\mu_{\rm ast}/r^2\sin\lambda\sin\varphi$, should always be positive in that cos$\theta \in [-1, 1]$. It indicates that the angles λ and φ must have the same sign. According to the definitions of these two angles, the corresponding situation is that the spacecraft and the Sun must lie on different sides of the asteroid's equatorial plane.

To accomplish body-fixed hovering, the required SRP acceleration in Equation (11) should be the same as that provided in Equation (4)

$$\Pi = \boldsymbol{a}^s_{\rm SRP} - \boldsymbol{a}^s\left(t\right) = C_2\cdot C_1\left(t\right)\cdot \boldsymbol{a}_{\rm SRP} - \boldsymbol{a}^s\left(t\right) = 0. \tag{14}$$

There are three control variables (β, α, δ) corresponding to the above three dimensional nonlinear equations. It is impossible to obtain analytical solutions but they can be solved numerically. For a specified position as expressed in Equation (9), if there is a set of quantities that vary with time (β, α, δ) making Equation (14) zero when θ_1 takes all values of 0 to 2π, the hovering orbit is feasible and vise versa. The nonlinear equations can be solved using Matlab's *'fsolve'* function with a default method of *'dogleg.'* In order to improve the calculation efficiency, a program from Minpack-1 (More et al. 1980), written in C++ (Jiang et al. 2012), is adopted to solve the nonlinear equations. In all simulations, the tolerance of Equation (14) is set to be better than 10^{-9}. Since Equation (14) is only three dimensional and is not a differential equation, it is not sensitive to initial values.

During the simulations when θ_1 takes all values from 0 to 2π, there are some "bad" cases that need to be verified. These correspond to feasible solutions (i.e. $0 < \beta \leq \beta_{\max}$, $||\alpha|| \leq \pi/2$). Specifically, the angles used for attitude control must be in their feasible domains. There are two cases that have arisen in our simulation process which can be transformed into feasible solutions. These two cases and their equivalent expressions are

$$\begin{cases} \alpha \in (-\pi/2,\, 0] \\ \delta > 0 \end{cases} \Rightarrow \begin{cases} \alpha = \|\alpha\| \\ \delta = \bmod\left(\pi + \delta,\, 2\pi\right) \end{cases}, \quad \begin{cases} \alpha \in [0,\, \pi/2) \\ \delta \in [-2\pi,\, 0] \end{cases} \Rightarrow \begin{cases} \alpha = \alpha \\ \delta = \bmod\left(2\pi + \delta,\, 2\pi\right) \end{cases}, \tag{15}$$

where the function 'mod' represents modulus after division.

3 CASE STUDY

The effects of sail coefficients, the angular velocity of the asteroid and the sail's area-to-mass ratio on the feasible region for body-fixed hovering are examined in this section. The influence of the hovering radius on controlling the sail is investigated through numerical simulations. The main parameters related to the asteroid are the same as those given by Williams & Abate (2009). The heliocentric orbit of the asteroid is assumed to be circular at 2.7 AU. Its diameter is 1.0 km with a density of 2.4×10^3 kg m^{-3} and its rotational period is 9.0 h with the spin axis aligned with the axis $+oz$. The highest lightness number is 0.153 corresponding to an area-to-mass ratio of 10 g m^{-2}. The solar latitude angle is set to be 60° for such a main-belt asteroid. Unless mentioned otherwise, all simulations in this section use these parameters.

3.1 Effect of Solar Sail Force Coefficients

Figure 2 shows the feasible regions where body-fixed hovering can occur with four different sail models whose coefficients are already given in Table 1. Since the asteroid is assumed to be spherically symmetric, feasible regions for θ_0 from 0 to 2π should be the same. Those feasible regions are located in the asteroid's northern hemisphere since the Sun is below its equatorial plane ($\varphi = 60°$). The region corresponding to the SPT sail is the largest while the smallest is the parametric case. The feasible regions of the optical and parametric sails are nearly the same although their model coefficients are totally different.

For those four sail models, all regions start from the corresponding synchronous points in the equatorial plane at a radius of $r_{\rm syn}$ ($r_{\rm syn} = \sqrt[3]{\mu_{\rm ast}/\omega^2}$, here $r_{\rm syn} \approx 1.31\,{\rm km}$). When the spacecraft reaches the asteroid's northern pole, all SRP force is used to counterbalance the asteroid's gravitational force. For an ideal sail, it is easy to find that the closest hovering radius is

$$r_{\rm min} = \sqrt{\frac{\mu_{\rm ast}}{\beta_{\rm max}\cdot(\mu_{\rm Sun}/R_{\rm AU}^2)\cdot\sin^2\varphi}}, \tag{16}$$

whose value in our case is approximately 0.95 km. The value of $r_{\rm min}$ for optical and parametric sails is 1.03 km while it is 0.88 km for the SPT sail. As a rough estimation, an efficiency factor of 0.85 can be added to Equation (6) to approximate the optical and parametric models here (see results from Williams & Abate 2009). The effect of a shadow from the asteroid with respect to the Sun is neglected, which reduces the effective hovering region for such a spherical model. For other irregularly shaped asteroids, such an effect needs to be discussed in detail.

3.2 Spinning Effects of the Asteroid

Figure 3 illustrates the effect of the spinning rate of the asteroid on the hovering regions with the asteroid at the lower center. Two spin angular velocities are considered, i.e. 9 h and 15 h (which is arbitrarily selected to be longer than 9 h). Only the ideal sail model is adopted here and that is why the minimum anti-Sun pole radius $r_{\rm min}$ is the same at 0.95 km. For the hypothetical case of slow spinning, the radius of the synchronous orbit is approximately 1.84 km. There is an overlapping area between the two regions when the hovering latitude angle λ is greater than 0.205π. The feasible region for hovering with a lower ω is a little larger than the higher case with a higher one. It indicates that there are more options for hovering positions (but with a relatively farther hovering radius at the same latitude) around slowly spinning asteroids compared to those with similar physical properties and orbital parameters.

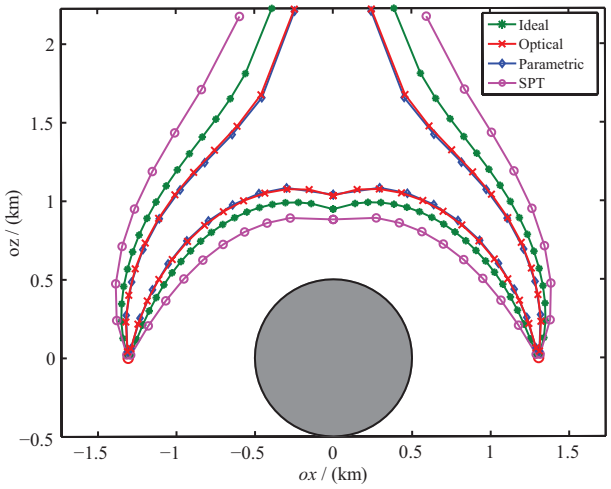

Fig. 2 Feasible regions for body-fixed hovering around an idealized spherical asteroid for four different sail models.

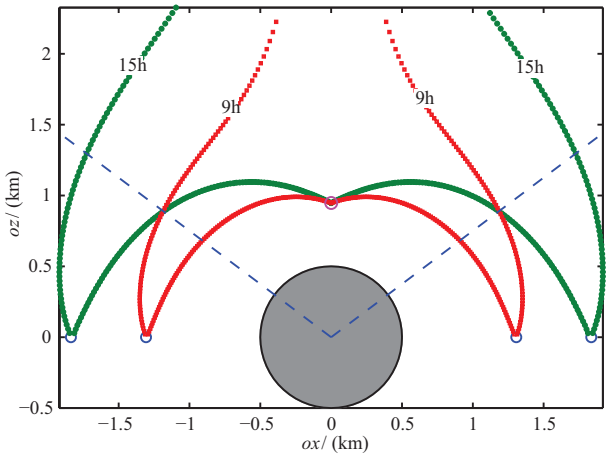

Fig. 3 Effect of the asteroid's spinning rate on the feasible region where hovering can occur.

3.3 Effect of the Area-to-Mass Ratio

In this subsection, the effect of the sail's area-to-mass ratio $\sigma(t)$ on the hovering radius will be investigated. According to recent studies, a characteristic acceleration on the order of 0.5 mm s^{-2} can be accomplished in near-term sail missions while a relatively mid-term square sail with a side length of 160 m has been envisaged by NASA for the *Solar Polar Imager* (*SPI*) mission (Mengali & Quarta 2009). The characteristic acceleration a_c is defined as the maximum acceleration produced by the sail at 1 AU when the normal direction with respect to the sail is parallel to the direction of sunlight. Thus, the lower limit for $\sigma_{\min}$ is 10 g m^{-2} corresponding to a near-term sail with $a_c = 0.91$ mm s^{-2}. The upper limit for $\sigma_{\min}$ is 4 g m^{-2} whose a_c is approximately 2.27 mm s^{-2}. For a sail with a variable sail area, the minimum area-to-mass ratio $\sigma_{\min}$ corresponds to the highest sail lightness number based on Equation (7). The values that have been investigated for $\sigma_{\min}$ ($\beta_{\max}$, a_{cmax}) are given in Table 2 along with their corresponding minimum hovering radii. These four

Table 2 Minimum Hovering Radius for Different Values of the Area-to-mass Ratio

$\sigma_{\min}$ (g m^{-2})	4	6	8	10
$\beta_{\max}$	0.3825	0.2550	0.1913	0.1530
a_{cmax} (mm s^{-2})	2.2682	1.5122	1.1344	0.9073
$r_{\min}$ (km)	0.599	0.734	0.848	0.947

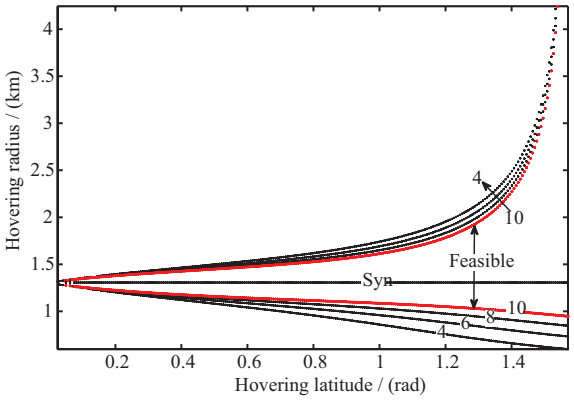

Fig. 4 Relation between hovering radius and latitude for different sail area-to-mass ratios.

values are enough to illustrate the influence of $\sigma_{\min}$ on the feasible regions where hovering can occur. Additionally, the minimum hovering radius for $\sigma_{\min} = 4$ g m^{-2} is 0.599 km, which is only 100 m away from the asteroid's surface. There is no need to be closer for an observation mission for such an idealized asteroid.

Figure 4 shows the variation of the hovering radius with respect to the hovering latitude in terms of each area-to-mass ratio. The curves above the synchronous orbit, with radius 1.31 km, are the outer boundaries of each feasible region while the curves below are the inner boundaries. The radius for body-fixed hovering is obtained by varying the hovering latitude in steps of 0.002π. It is easy to find that the feasible region for $\sigma_{\min} = 4$ g m^{-2} is larger than the other three cases due to its higher characteristic acceleration. The biggest gap in hovering radius between different values of $\sigma_{\min}$ in Figure 4 occurs at the asteroid's polar region with a value of 0.35 km from Table 2.

Body-fixed hovering for different latitudes with respect to the asteroid is feasible by using a solar sail. When the hovering latitude is specified, an increase of $\sigma_{\min}$ in the above scenarios can increase the hovering boundaries a little, especially for areas away from the polar region. For example, if the hovering latitude λ is 0.264π, the inner boundary for $\sigma_{\min} = 4$ g m^{-2} is 0.94 km while it is 1.11 km for $\sigma_{\min} = 10$ g m^{-2}. A decrease in hovering height of 170 m for $\sigma_{\min} = 10$ g m^{-2} allows the mass of the spacecraft to be 2.5 times larger than for the case of $\sigma_{\min} = 4$ g m^{-2}, which indicates that there is a tradeoff between the hovering radius and the mass of the spacecraft. Taking the 160 m^2 sail in the proposed *SPI* mission as an example, the payload mass of the spacecraft for $\sigma_{\min} = 10$ g m^{-2} is 256 kg. By contrast, the payload mass for $\sigma_{\min} = 4$ g m^{-2} is only 102 kg. Therefore, it is preferable to have more mass with low-performance sails to accomplish a mission that requires body-fixed hovering.

3.4 Effect of the Hovering Radius

The effect of the hovering radius on the sail control profile will be examined in this subsection. Without loss of generality, the hovering latitude is set to be $\pi/4$ and the minimum sail area-to-mass ratio is 10 g m^{-2}. The boundary values for this hovering latitude are 1116 m and 1522 m. Three

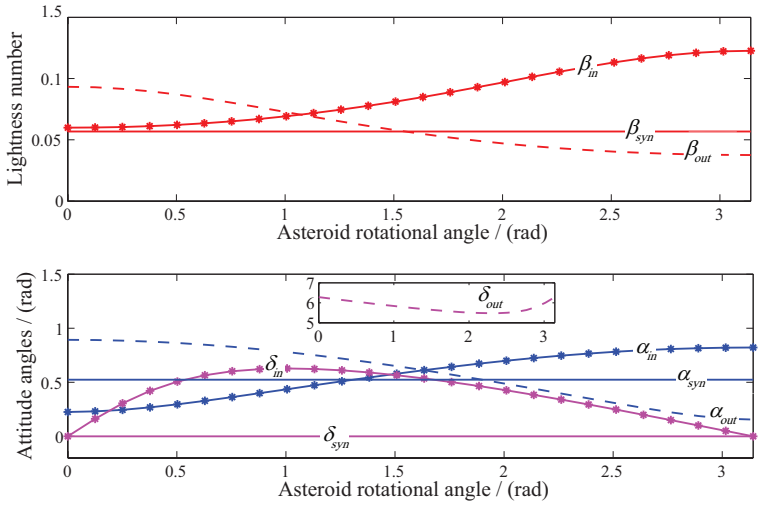

Fig. 5 Solar sail control profile in the first half period for different hovering radii (in: 1156 m; syn: 1306 m; out: 1456 m).

hovering radii are investigated, i.e. 1156 m, 1306 m and 1456 m, where 1306 m is the synchronous radius and the two others are in the feasible region, 150 m away from the synchronous orbit. Since the incident light frame *IXYZ* is assumed to be non-rotating, the sail control profile for body-fixed hovering is symmetrical with respect to the *IXZ* plane. Let us assume there are $2n$ + 1 discrete points in the control profile between 0 to 2π where n is an integer. In the current simulations, n is 500, corresponding to a calculation step of 0.002π for spinning of the asteroid. Then, the control variables after π can be obtained as

$$\begin{cases} \beta\,(n+1) \;=\; \beta\,(n-1)\;, \\ \alpha\,(n+1) \;=\; \alpha\,(n-1)\;, \\ \delta\,(n+1) \;=\; 2\pi - \delta\,(n-1)\;. \end{cases} \tag{17}$$

The sail control profile in the first half period is shown in Figure 5 for each case, including the sail lightness number and two attitude angles for the sail. To distinguish orientations of the sail in the bottom plot of Figure 5, the clock angle $\delta_{\rm out}$ for the outward case (1456 m) is shown separately. For all these three cases, the peak in the lightness number does not exceed the maximum value of 0.153. For both the inward (1156 m) and outward cases, the lightness number and attitude angles of the sail vary with time to fulfill the requirement of non-synchronous body-fixed hovering.

It is interesting that the clock angle $\delta_{\rm syn}$ is always zero for the synchronous case (1306 m with $\lambda = \pi/4$) while the control variables $\beta_{\rm syn}$ and $\alpha_{\rm syn}$ are constant. This result indicates that the required acceleration from the sail is only provided to counterbalance the asteroid's gravitational acceleration along the axis *IZ*. Such a condition can be explicitly deduced for an ideal sail from Section 2.2. For a body-fixed hovering position at a synchronous height out of the equatorial plane, the required acceleration from the sail in Equation (11) is simplified to

$$\boldsymbol{a}_{\rm syn} = \left[\, 0,\; 0,\; \frac{\mu_{\rm ast}}{r_{\rm syn}^2}\sin\lambda \,\right]^{\rm T}. \tag{18}$$

Substituting Equation (5) into Equation (6) with δ = 0, one can obtain

$$\boldsymbol{a}^s\,(t) = \beta\,(t)\cdot\frac{\mu_{\rm Sun}}{R_{\rm AU}^2}\cdot\cos^2\alpha\cdot\begin{bmatrix}\cos\alpha\\ 0\\ \sin\alpha\end{bmatrix}. \tag{19}$$

In order to guarantee the feasibility of body-fixed hovering, the acceleration from the sail acceleration provided by Equation (19) should be equal to that required in Equation (18). Therefore, the sail cone angle must satisfy $\alpha = \pi/2 - \varphi$ to make sure that the acceleration from the sail is along the *+IZ* direction. In such a case, the required lightness number can be obtained as

$$\beta_{\rm syn} = \frac{\mu_{\rm ast}}{\mu_{\rm Sun}} \cdot \frac{R_{\rm AU}^2}{r_{\rm syn}^2} \cdot \frac{\sin\lambda}{\sin^2\varphi}. \tag{20}$$

For the above case, the lightness number for the sail can be calculated from Equation (20) as 0.057, which is consistent with the value shown in Figure 5. It is interesting that body-fixed hovering above the asteroid can be accomplished by using solar sailing with constant values of control variables at the synchronous radius out of the equatorial plane. Such a property would be very attractive for future missions that need body-fixed hovering. First, the spinning periods of asteroids are usually different in different asteroids. Second, attitude control with a sail made from a large thin film is very challenging and complicated (Wie & Murphy 2007; Gong et al. 2009b). Therefore, for specified hovering latitudes out of the asteroid's equatorial plane, a spacecraft placed at the height of the synchronous orbit can maintain a fixed position with a constant attitude and lightness number.

For idealized spherical asteroids, gravitational accelerations from perturbations of other celestial bodies are also ignored in this study. In fact, they may play a key role in the stability of a hovering orbit. Moreover, the variations in the Sun-asteroid distance due to the eccentric orbits of asteroids should have a great influence on the dynamics of the hovering orbit (Farrés & Jorba 2012). All the above effects should be taken into account in future studies. The stability of these hovering orbits and their controllability will be the subject of the next work that we will publish. In terms of diverse shapes of the asteroids, a study of hovering around elongated asteroids is in progress based on the current framework.

4 CONCLUSIONS

Feasible regions for body-fixed hovering over an asteroid have been investigated by using solar sails. Four different sail models with an active sail area are considered including cases of ideal, optical, parametric and SPT sails. Nonlinear equations are constructed to obtain the feasible region for hovering and numerical solutions are obtained. With advanced thrust ability, the SPT sail can produce the largest hovering region, but the region shrinks for other sails. For the inner and outer boundaries of the hovering radius, the effect of nonideal models must be considered in planning the mission. The spinning rate of the asteroid plays a key role in characteristics of the feasible region for hovering. With the same physical and orbital characteristics, an asteroid with a longer spinning period (in our study, the period of 15 h corresponds to a slowly spinning asteroid) yields a larger feasible region than the one with a shorter period (9 h). For a desired hovering position away from the synchronous orbit, both the lightness number of the sail and its attitude have to be adjusted to counterbalance the asteroid rotation with gravitational acceleration out of the equatorial plane. For hovering positions at the height of the synchronous orbit out of the equatorial plane, acceleration from the sail is only provided to counterbalance gravitational acceleration, resulting in a constant sail attitude and lightness number. Such a property is very attractive for missions that need body-fixed hovering with a solar sail. This approach will be extended to asteroids with different shapes in future studies.

Acknowledgements This work was supported by the National Basic Research Program of China (973 Program, 2012CB720000) and the Tsinghua University Initiative Scientific Research Program (No. 20131089268). We thank Dr. Jin-Guang Li for his help using Latex.

References

Baoyin, H., & McInnes, C. 2005, Journal of Guidance Control Dynamics, 28, 1328
Baoyin, H., & McInnes, C. R. 2006, Journal of Guidance Control Dynamics, 29, 538
Broschart, S. B., & Scheeres, D. J. 2005, Journal of Guidance Control Dynamics, 28, 343
Farrés, A., & Jorba, À. 2012, in Proceedings of the 63rd International Astronautical Congress, Italy (IAC-12.C1.6.4)
Gong, S., Baoyin, H., & Li, J. 2007, Journal of Guidance Control Dynamics, 30, 1148
Gong, S., Li, J., & Baoyin, H. 2009a, Celestial Mechanics and Dynamical Astronomy, 105, 159
Gong, S., Baoyin, H., & Li, J. 2009b, Acta Astronautica, 65, 730
Gong, S.-P., Li, J.-F., & Gao, Y.-F. 2011, RAA (Research in Astronomy and Astrophysics), 11, 205
Guerman, A. D., Smirnov, G. V., & Pereira, M. C. 2010, Mathematical Problems in Engineering, 2009
Hu, W.-D., & Scheeres, D. J. 2008, ChJAA (Chin. J. Astron. Astrophys.), 8, 108
Jiang, F., Li, J., & Baoyin, H. 2012, Journal of Guidance Control Dynamics, 35, 245
Li, X., Qiao, D., & Cui, P. 2013, Ap&SS, 348, 417
McInnes, C. R. 1999, Solar Sailing. Technology, Dynamics and Mission Applications, by McInnes, C. R. (London: Springer)
Mengali, G., & Quarta, A. A. 2007, Acta Astronautica, 60, 676
Mengali, G., & Quarta, A. A. 2009, Journal of Spacecraft and Rockets, 46, 134
More, J., Garbow, B., & Hillstrom, K. Argonne National Laboratory, 1980, *http://www.netlib.org/minpack* [retrieved 22 Feb. 2015]
Morrow, E., Scheeres, D., & Lubin, D. 2001, Journal of Spacecraft and Rockets, 38, 279
Morrow, E., Scheeres, D. J., & Lubin, D. 2002, AIAA, 4994, 1
Sawai, S., Scheeres, D. J., & Broschart, S. B. 2002, Journal of Guidance Control Dynamics, 25, 786
Scheeres, D. J. 1999, JAS, 47, 25
Scheeres, D. J. 2004, in Planetary Defense Conference, Orange County, California, 23rd Feb, 2004-1445
Scheeres, D. J., Ostro, S. J., Hudson, R. S., DeJong, E. M., & Suzuki, S. 1998, Icarus, 132, 53
Vulpetti, G. 1997, Acta Astronautica, 40, 733
Wie, B., & Murphy, D. 2007, Journal of Spacecraft and Rockets, 44, 809
Williams, T., & Abate, M. 2009, Journal of Spacecraft and Rockets, 46, 967
Zhang, J., Zhao, S., & Yang, Y. 2013, Aerospace and Electronic Systems, IEEE Transactions on, 49, 2742